GEOPHYSICS, VOL. 81, NO. 6 (NOVEMBER-DECEMBER 2016); P. D573–D584, 9 FIGS., 1 TABLE.
10.1190/GEO2016-0088.1




DOI:10.1190/geo2016-0088.1

# Effective fluid and grain bulk moduli for heterogeneous thinly layered poroelastic media

Uri Wollner[1] and Jack Dvorkin[1]

## ABSTRACT

Consider a package of parallel porous layers in which the porosity, the bulk modulus of the pore fluid, and the bulk modulus of the mineral phase are constant within each layer but may vary along the package. We wished to apply Gassmann's fluid substitution to the entire package now treated as an effective medium (long-wavelength case). The question is: What are the effective properties, namely, the mineral's and fluid's bulk moduli, to be used in this operation? The answer depends on the degree of hydraulic communication between the layers. We have examined two limiting cases: (1) all layers in the package are in perfect communication and (2) all layers are hydraulically isolated from each other. The two mathematical methods relevant to these cases are (1) the poroelastic Backus average for the former and (2) the elastic Backus average, respectively. By conducting a sufficient number of numerical experiments, we have found that, in both cases, the effective mineral bulk modulus for the package is very close to the value of the Hill's average of the bulk moduli of individual layers weighted by their solid fraction. In the case of perfect hydraulic communication, the effective fluid bulk modulus is very close to the harmonic average of the individual moduli weighted by individual porosity. For the case of hydraulically isolated layers, the effective fluid bulk modulus falls between the porosity-weighted harmonic and arithmetic averages. We have evaluated approximate close-form solutions for both cases and found that these approximations cause less than 6% average relative error in the computed stiffness components. Bearing in mind that the full communication and complete isolation scenarios are relevant to very low- and very high-frequency wave propagation, respectively, our results can be interpreted as the frequency dispersion of the effective fluid bulk modulus.

## INTRODUCTION

Subsurface imaging and estimation of petrophysical parameters (Avseth et al., 2005; Symes, 2008; Virieux and Operto, 2009) are partially based on interpretation of a medium's response to an incident wave. As the wavelength of the incident wave shortens, one may obtain better resolved features of the subsurface. Features such as alternating layers of sand and shale are not uncommon (Avseth et al., 2001; Dejtrakulwong, 2012). If the ratio between the wavelength $\lambda$ and the average layer thickness $d$ is such that

$$\lambda/d \gg 1 \tag{1}$$

the medium can be described as an effective medium. A layered sequence pertaining to this so-called long wavelength limit is often called finely layered. The effects of unresolved layers on the effective medium contribute to velocity anisotropy and apparent attenuation (scattering) of elastic waves (Backus, 1962; Morlet et al., 1982; Marion et al., 1994; Sams, 1995). Conversely, at the limit $d/\lambda \gg 1$, wave propagation within a layered sequence occurs along a raypath, following Fermat's principle (also known as ray theory). At intermediate scales, apparent attenuation due to interference of multiple reflections has been reported numerically and experimentally (Schoenberger and Levin, 1978; Morlet et al., 1982; Marion et al., 1994).

Backus (1962) shows that finely layered media composed of isotropic (or transversely isotropic) linearly elastic materials can be represented as an effective medium having transversely isotropic symmetry. This derivation assumed that the layers are in welded contact. Hence, if the direction of layering is the $x_3$-direction, in-plain strains (i.e., $e_{11}$, $e_{22}$, and $e_{12} = e_{21}$) are continuous; otherwise, the layers would experience relative slip. In addition, it follows from the welded contact interface assumption that the stresses acting along the planes parallel to the layering are the same (i.e.,

Manuscript received by the Editor 17 February 2016; revised manuscript received 21 June 2016; published online 7 September 2016.
[1]Stanford University, Department of Geophysics, Stanford, California, USA. E-mail: uriwolln@stanford.edu; dvorkin@stanford.edu.

DOI:10.1190/geo2016-0088.1

$\sigma_{13} = \sigma_{31}$, $\sigma_{23} = \sigma_{32}$, and $\sigma_{33}$ must be continuous as well; Postma, 1955; Schoenberg and Muir, 1989; Berryman, 1998). In this case, the effective medium has vertical transversely isotropic symmetry.

Gelinsky and Shapiro (1997) and Berryman (2011) extend finely layered averaging to linearly elastic porous medium (poroelastic) based on Biot's (1956a, 1956b, 1962) theory, incorporating frequency-dependent fluid interaction with the solid frame. Biot's model examines a homogeneous effective medium that is isotropic and linearly elastic. In addition, the model assumes that the medium has well-connected pore system, and it is fully saturated by a single fluid.

For poroelastic layered media, Gelinsky and Shapiro (1997) use self-averaging properties of seismic wavefield parameters to obtain the effective medium constants, whereas Berryman (2011) follows the approach of Schoenberg and Muir (1989) and applies it to the compliance form of the stress-strain relations for linearly elastic composites with the addition of fluid related terms. Berryman (2011) rearranges and partitions the stress-strain relations to distinguish between strain and stress terms that are uniform across a layered package to those that vary. This formulation allowed to perform volume averaging perpendicular to the layering direction for strains and stresses that are not continuous across layer boundaries.

Gelinsky and Shapiro (1997) and Berryman (2011) distinguish between two limits under the long-wavelength approximation: quasi-static and no-flow. Small displacement disturbances caused by wave propagation within a saturated porous medium can give rise to pressure disequilibrium in the fluid phase. In the quasi-static limit, the wave-induced pore-pressure differences have sufficient time to equilibrate across layer boundaries by interlayer flow, hence resulting in continuity of fluid pressure across the boundaries. On the other hand, incident waves with higher frequencies (i.e., shorter wavelengths that still satisfy the long-wavelength approximation) will inhibit pressure equilibration. Subsequently, at the no-flow limit, the layers behave as if they are hydraulically isolated from each other (undrained), which results in an increase in the propagation speed through the medium relative to the quasi-static case.

The most widely used tool for fluid substitution was developed by Gassmann (1951). Gassmann's anisotropic formulation predicts the response of rock with anisotropic dry frame composed of a single mineral and interconnected fluid-filled pores. Subresolution heterogeneity in the form of multimineralic components, anisotropic minerals, and/or partial hydraulic communication in thinly layered media violates Gassmann's assumptions. For the case of a single mineral composing all layers within a package, it is shown in Appendix A that the Gelinsky and Shapiro (1997) formulation for the quasi-static limit (low frequencies) reduces to Gassmann's anisotropic form. To correctly apply fluid substitution to a package of hydraulically disconnected thin layers, one must perform fluid substitution at each layer separately (assuming individual layers fulfill Gassmann's assumptions) and then determine the effective response through elastic Backus averaging (Katahara, 2004; Skelt, 2004). Another fluid-substitution scheme in sand-shale sequences was proposed by Dejtrakulwong and Mavko (2011), which assumes that the layers are hydraulically disconnected.

In this study, we derive approximate analytic expressions for the inputs to anisotropic Gassmann's fluid substitution for a layered package for hydraulically communicating and isolated cases. Our results for the effective bulk modulus of the pore fluid can be interpreted as the frequency dispersion of the effective fluid bulk modulus.

## BACKGROUND: ISOTROPY AND ANISOTROPY

### Isotropic symmetry

Isotropic symmetry requires two different parameters to describe a material. For instance, Lame's first parameter $\lambda$ and the shear modulus $\mu$. The corresponding stiffness matrix is given by

$$\begin{bmatrix} c_{11} & c_{12} & c_{12} & 0 & 0 & 0 \\ c_{12} & c_{11} & c_{12} & 0 & 0 & 0 \\ c_{12} & c_{12} & c_{11} & 0 & 0 & 0 \\ 0 & 0 & 0 & c_{44} & 0 & 0 \\ 0 & 0 & 0 & 0 & c_{44} & 0 \\ 0 & 0 & 0 & 0 & 0 & c_{44} \end{bmatrix}, \tag{2}$$

with $c_{11} = \lambda + 2\mu$, $c_{12} = \lambda$, and $c_{44} = \mu$.

### Transversely isotropic symmetry

The term transverse isotropy (TI) is slightly misleading as, in fact, it defines an anisotropic medium. The isotropy is limited to the "transverse" plane (Thomsen, 1986). A TI material is described by five different stiffness constants. The stiffness tensor of a TI medium with vertical ($x_3$-direction) symmetry axis (VTI) is given by

$$\begin{bmatrix} c_{11} & c_{12} & c_{13} & 0 & 0 & 0 \\ c_{12} & c_{11} & c_{13} & 0 & 0 & 0 \\ c_{13} & c_{13} & c_{33} & 0 & 0 & 0 \\ 0 & 0 & 0 & c_{44} & 0 & 0 \\ 0 & 0 & 0 & 0 & c_{44} & 0 \\ 0 & 0 & 0 & 0 & 0 & c_{66} \end{bmatrix}, \tag{3}$$

with $c_{66} = (c_{11} - c_{12})/2$.

## PROBLEM FORMULATION

We have a layered package in which each layer is isotropic and has its individual porosity $\phi$; mineral bulk and shear moduli $K_s$ and $\mu_s$, respectively; drained elastic bulk and shear moduli $K_{\text{dry}}$ and $\mu_{\text{dry}}$, respectively; and bulk modulus $K_f$. The effective drained (dry) stiffness matrix $\bar{c}^{\text{dry}}_{lm}$ $(l, m = 1, 2, \ldots, 6)$ of this package is computed by applying the Backus average to the dry elastic properties of individual layers (Appendix A). The effective porosity $\bar{\phi}$ is the volume average of individual porosities.

Then, for the layers with pore fluids, we need to select the method of computing the effective stiffness matrix. Here, we select two methods: (1) the poroelastic Backus-average method, in which it is assumed that the pore fluids in the layers are in perfect hydraulic communication, i.e., any wave-induced perturbations of local pore pressure equilibrate throughout the entire package within the oscillation period, relevant to the zero-frequency limit and (2) the purely elastic Backus-average method applied to saturated layers, in which the individual bulk moduli are obtained by applying isotropic Gassmann's fluid substitution to each layer, relevant to the infinite-frequency limit.

Our questions are: If we wish to apply anisotropic Gassmann's fluid substitution to the entire package treated as an effective medium, what should be the effective bulk moduli of the mineral phase and pore fluid of the upscaled effective medium to be used in this operation? The proposed method of obtaining the effective bulk

moduli of the mineral phase and pore fluid for a layered package having multimineralic components and/or partial hydraulic communication requires solving an over-determined system of equations. To mitigate this problem, we find an approximate solution and validate it by exhaustive forward modeling. The resulting average relative errors in the effective elastic stiffnesses do not exceed 6%.

## WORKFLOW: NUMERICAL EXPERIMENTS

### Setup

We constructed a layered package containing 100 layers by randomly (uniform distribution) varying the thickness of each layer in the package such that the total thickness of the package remained constant. Each layer was composed of two mineral components (one stiff and the other soft). The mineral bulk and shear moduli in each layer were computed as the Hill's average (Mavko et al., 2009) of those of the soft and the stiff mineral components: the bulk and shear moduli of the soft component were 21.0 and 7.0 GPa (the Gulf clay, Mavko et al., 2009), respectively, whereas these values for the stiff component were 76.8 and 32.9 GPa (calcite). The fraction of the soft mineral was randomly selected from a uniform distribution in the range of 0.00–1.00. The porosity of each layer was also randomly assigned between 0.05 and 0.35 using a uniform distribution. The dry-frame elastic properties (isotropic) for each layer were then computed from the porosity and the mineral bulk and shear moduli using the soft-sand model or, separately, the stiff-sand model with a constant coordination number of six, differential pressure of 12 MPa, critical porosity of 0.4, and shear stiffness correction factor of one, meaning that the grain-to-grain shear stiffness at critical porosity was given by the Hertz-Mindlin contact model (Mavko et al., 2009).

### Experiments

We explored the upscaled effective medium properties of 1000 thinly layered packages with layering perpendicular to the $x_3$-direction. Because each layer was isotropic, the effective elastic anisotropy of a package had VTI symmetry.

Initially, we determined the five independent effective dry-frame stiffness matrix components $\bar{c}_{lm}^{\text{dry}}$ by applying the elastic Backus average to an entire package using the dry-frame elastic moduli of individual layers.

In the following numerical experiments, we assumed that the effective porosity of a package $\bar{\phi}$ was the volume average of individual porosities:

$$\bar{\phi} = \langle \phi \rangle, \tag{4}$$

where $\langle \cdot \rangle$ is the averaging operator across all layers. For instance, given material quantity $\mathbf{m}$, its average value for a stack of $N$ layers is given by $\bar{\mathbf{m}} = \langle \mathbf{m} \rangle = \sum_{k=1}^{N} f^{(k)} \mathbf{m}^{(k)}$ with $f^{(k)}$ and $\mathbf{m}^{(k)}$ being the volumetric fraction and the material quantity of the $k$th layer, respectively. The volumetric fraction satisfies $\sum_{k=1}^{N} f^{(k)} = 1$.

The purpose of the first experiment was to determine the Gassmann-consistent effective mineral bulk modulus $\bar{K}_s$ for an entire package to be used in Gassmann's anisotropic fluid substitution. To do this, we filled all layers with the same fluid so that the fluid bulk modulus $K_f$ to be used in fluid substitution was known and fixed (i.e., the effective fluid $\bar{K}_f$ equals $K_f$). First, we assumed that all layers were in perfect hydraulic communication (quasi-static limit) and determined the exact effective undrained stiffness components $\bar{c}_{lm}^{\text{QS}}$ by using the poroelastic Backus average (Gelinsky and Shapiro, 1997) with equations listed in Appendix A. Then, we found $\bar{K}_s$ for the entire package by requiring that $\bar{c}_{lm}^{\text{QS}}$ matched the undrained stiffness components predicted from the dry-effective medium using anisotropic Gassmann's fluid substitution,

$$\begin{aligned}
\bar{c}_{KL}^{\text{Gass}} &= \bar{c}_{KL}^{\text{dry}} + \beta_K \beta_L \bar{M}; \quad K, L = 1, 2, 3, \\
\bar{c}_{44}^{\text{Gass}} &= \bar{c}_{44}^{\text{dry}}; \quad \bar{c}_{66}^{\text{Gass}} = \bar{c}_{66}^{\text{dry}}, \\
\bar{M} &= \left[ \frac{\bar{\phi}}{\bar{K}_f} + \frac{\bar{\alpha} - \bar{\phi}}{\bar{K}_s} \right]^{-1}, \\
\beta_J &= 1 - \frac{\bar{c}_{1J}^{\text{dry}} + \bar{c}_{2J}^{\text{dry}} + \bar{c}_{3J}^{\text{dry}}}{3\bar{K}_s},
\end{aligned} \tag{5}$$

with the effective-stress coefficient

$$\bar{\alpha} = 1 - \frac{\sum_{K=1}^{3} \sum_{L=1}^{3} \bar{c}_{KL}^{\text{dry}}}{9\bar{K}_s}. \tag{6}$$

Note that the fluid-dependent term $\bar{M}$ does not affect the undrained shear-stiffness components of the medium. Therefore, $\bar{c}_{44}^{\text{Gass}}$ and $\bar{c}_{66}^{\text{Gass}}$ are equivalent to the exact solution using the poroelastic Backus averaging. In addition, as the effective medium has VTI symmetry, it follows that $\bar{c}_{11}^{\text{Gass}}$ can be expressed as $\bar{c}_{11}^{\text{Gass}} = 2\bar{c}_{66}^{\text{Gass}} + \bar{c}_{12}^{\text{Gass}}$. Therefore, due to the symmetry of the stiffness matrix, the expression in equation 5 gives three separate conditions on the effective mineral modulus $\bar{K}_s$ (i.e., for $\bar{c}_{12}^{\text{Gass}}$, $\bar{c}_{13}^{\text{Gass}}$, and $\bar{c}_{33}^{\text{Gass}}$). If the upscaled $\bar{c}_{ij}^{\text{QS}}$ $(ij = 12, 13, 33)$ moduli were exactly Gassmann consistent, then a single $\bar{K}_s$ would satisfy all three conditions. In the case of multimineralic composites, the two models are not equivalent, so the system is overdetermined, and at best we can only find the optimum $\bar{K}_s$ that minimizes the difference between the undrained stiffness constants of the two models' predictions. We found that matching each of the undrained stiffness constants produced a different $\bar{K}_s$ (Figure 1), and we compared them with the Voigt $K_{sV\phi}$ and the Reuss $K_{sR\phi}$ averages weighted by the solid fraction (i.e., $1 - \phi$) in each layer,

$$K_{sV\phi} = \frac{1}{\langle 1 - \phi \rangle} \langle (1 - \phi) K_s \rangle, \tag{7}$$

$$K_{sR\phi} = \left( \frac{1}{\langle 1 - \phi \rangle} \left\langle \frac{(1 - \phi)}{K_s} \right\rangle \right)^{-1}, \tag{8}$$

and to their mean (Hill's average),

$$K_{sH\phi} = \frac{K_{sV\phi} + K_{sR\phi}}{2}. \tag{9}$$

To ignore the situation of an overdetermined system, we simply assumed that $\bar{K}_s = K_{sH\phi}$. To justify this assumption, we computed the three $\bar{c}_{ij}^{\text{Gass}}$ from anisotropic Gassmann's fluid substitution using this $\bar{K}_s$ and the uniform $\bar{K}_f$ and then compared these stiffnesses with the exact $\bar{c}_{ij}^{\text{QS}}$ as given by the poroelastic Backus average

(Figure 2). We conducted this experiment for two extreme $\bar{K}_f$ values, 0.05 and 3.00 GPa, and we found that the average difference between $\bar{c}_{ij}^{\text{Gass}}$ and $\bar{c}_{ij}^{\text{QS}}$ was less than 2% (first and second columns). The average relative errors and their respective standard deviations in percentage $\bar{\Delta}\bar{c}_{ij}$ are listed in each plot.

The purpose of the second experiment was to determine the effective fluid bulk modulus $\bar{K}_f$ to be used in Gassmann's fluid substitution to match the poroelastic Backus average $\bar{c}_{ij}^{\text{QS}}$ in cases in which the fluid varied between the layers. For this purpose, we populated each layer with a different fluid, whose bulk modulus was randomly selected from a uniform distribution between 0.05 and 3.00 GPa. In Gassmann's fluid substitution, we used $\bar{K}_s$ given in equation 9. Once again, as in the mineral bulk modulus case, we faced an overdetermined system of equations and, to address it, we assumed that $\bar{K}_f$ is the porosity-weighted harmonic (Reuss) average of individual fluid bulk moduli,

$$K_{fR\phi} = \left(\frac{1}{\langle\phi\rangle}\left\langle\frac{\phi}{K_f}\right\rangle\right)^{-1}. \tag{10}$$

The average relative difference between $\bar{c}_{ij}^{\text{QS}}$ and $\bar{c}_{ij}^{\text{Gass}}$ with this choice of $\bar{K}_f$ did not exceed 2% (Figure 2, third column). Another possibility was to compute $\bar{K}_f$ similar to equation 10 but without weighting by porosity (Figure 2, fourth column):

$$K_{fR} = \left\langle\frac{1}{K_f}\right\rangle^{-1}, \tag{11}$$

which produced a greater average difference standard deviation (approximately 4%) compared with using equation 10.

The first and second experiments were repeated for the case, where the layers were hydraulically isolated from each other (no-flow limit). The exact effective stiffness components $\bar{c}_{ij}^{\text{NF}}$ were found by applying the elastic Backus average to the package in which the individual elastic properties were obtained by isotropic Gassmann's fluid substitution in each layer (Appendix A). For the two cases of uniform $K_f$, the three $\bar{c}_{ij}^{\text{Gass}}$ determined from anisotropic Gassmann's fluid substitution using $\bar{K}_s = K_{sH\phi}$ and $\bar{K}_f = K_f$ were compared with the exact stiffness components values (Figure 3, first and second columns). The average relative differences and their respective standard deviations in percentage $\Delta\bar{c}_{ij}$ are shown in each plot. The maximum average difference in stiffnesses was less than 3% using $\bar{K}_s = K_{sH\phi}$. Therefore, $\bar{K}_s = K_{sH\phi}$ was subsequently used in the experiments where $K_f$ varied among the layers.

In the case of varying fluid bulk moduli among the layers, the $\bar{c}_{ij}^{\text{Gass}}$ computed using $\bar{K}_f$ either from equation 10 or 11 did not match the exact values (Figure 3, the last two columns). As before, $\bar{K}_f$ could be independently found by matching three effective stiffnesses: $\bar{c}_{12}^{\text{Gass}}$, $\bar{c}_{13}^{\text{Gass}}$, and $\bar{c}_{33}^{\text{Gass}}$. To address the issue of an over-determined system, we found $\bar{K}_f$ that minimized the error in the least-squares sense among $\bar{c}_{12}^{\text{NF}}$, $\bar{c}_{13}^{\text{NF}}$, and $\bar{c}_{33}^{\text{NF}}$ and their respective effective stiffnesses obtained using anisotropic Gassmann's fluid substitution. This $\bar{K}_f$ fell between the Reuss $K_{fR\phi}$ and Voigt $K_{fV\phi}$ bounds weighted by porosity for the individual fluid bulk moduli (Figure 4, left column) with the respective bounds given by the following equation:

$$K_{fR\phi} \equiv \left(\frac{1}{\langle\phi\rangle}\left\langle\frac{\phi}{K_f}\right\rangle\right)^{-1} < \bar{K}_f < \frac{1}{\langle\phi\rangle}\langle\phi K_f\rangle \equiv K_{fV\phi}. \tag{12}$$

Assuming that $\bar{K}_f$ can be approximated using a linear combination of $K_{fR\phi}$ and $K_{fV\phi}$,

$$\bar{K}_f = aK_{fR\phi} + bK_{fV\phi}. \tag{13}$$

We empirically found that the coefficients to be used in the soft-sand model are $a = 0.27$ and $b = 0.68$, whereas in the stiff-sand model, the coefficients are $a = 0.15$ and $b = 0.86$. To validate these relations, we calculated $\bar{c}_{ij}^{\text{Gass}}$ and compared them with the exact $\bar{c}_{ij}^{\text{NF}}$. The results are shown in Figure 4 (middle column) along with

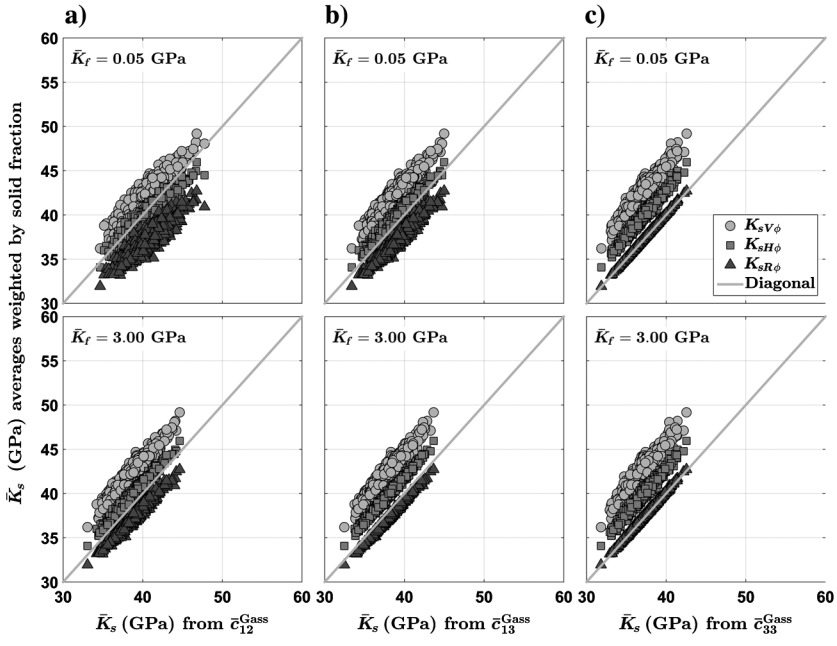


Figure 1. Realizations results using the soft-sand model for fully communicating layers. Three values of $\bar{K}_s$ found using three different stiffness components as indicated on the horizontal labels in each plot. These are plotted versus those obtained by (a) Voigt $K_{sV\phi}$, (b) Reuss $K_{sR\phi}$, and (c) Hill's $K_{sH\phi}$ averages of the individual $K_s$ in each layer weighted by the solid fraction. The upper row is for uniform fluid with bulk modulus 0.05 GPa, and the lower row is for uniform fluid with 3.00 GPa. For both pore fluids, the $\bar{K}_s$ derived from $\bar{c}_{12}^{\text{Gass}}$ by many realizations qualitatively fall around Hill's average; $\bar{K}_s$ derived from $\bar{c}_{13}^{\text{Gass}}$ fall between Hill's and Reuss averages, whereas those from $\bar{c}_{33}^{\text{Gass}}$ fall upon Reuss average.

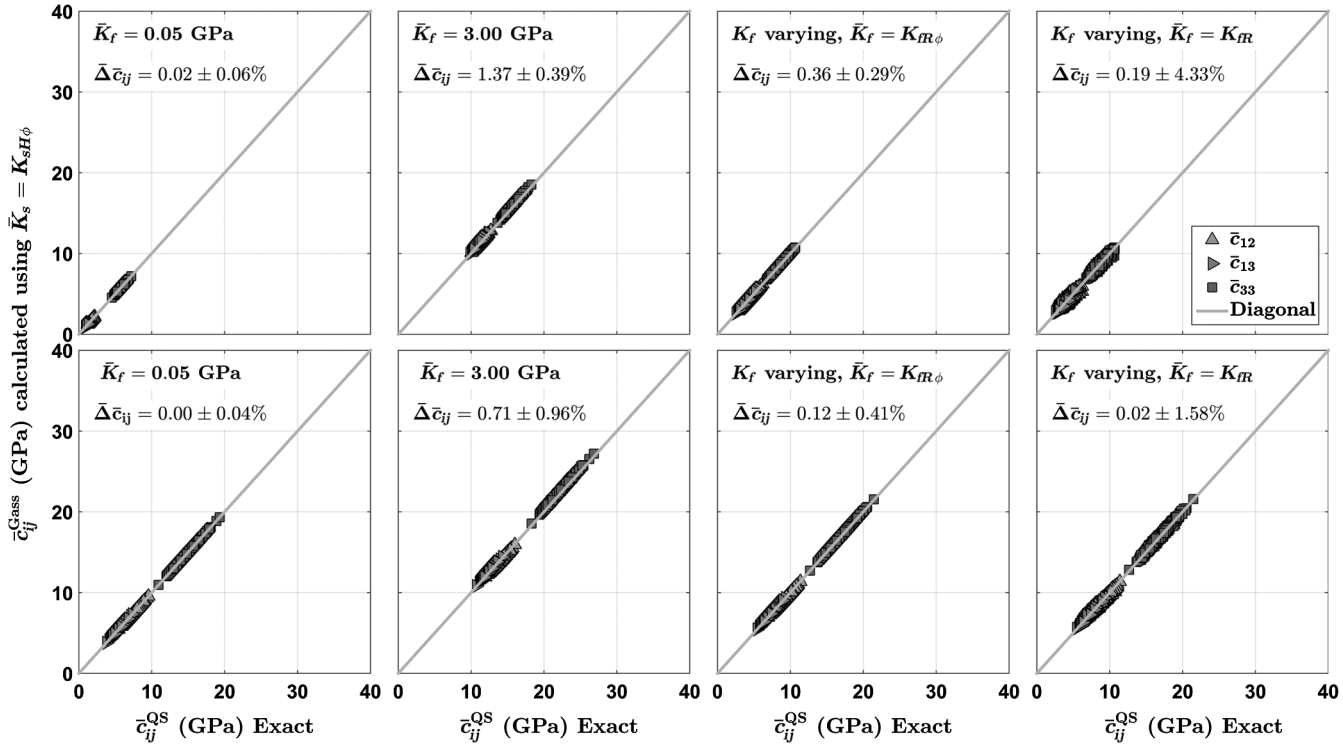


Figure 2. Fully communicating layers. Upper row: Soft-sand model. Three effective stiffnesses from anisotropic Gassmann's fluid substitution computed using $\bar{K}_s = K_{sH\phi}$ and the uniform $K_f$ (first two plots) plotted against exact poroelastic Backus stiffnesses. The same crossplot is shown in the third plot with the same $\bar{K}_s$ but now varying the fluid bulk modulus among the layers and using the effective fluid bulk modulus for the uniform fluid that is the porosity-weighted Reuss average of individual $K_f$ (equation 10). The same crossplot is in the fourth plot, but now using the effective fluid bulk modulus harmonically averaged among the layers but not weighted by individual porosity (equation 11). The average relative errors and their respective standard deviations in percentage $\bar{\Delta}\bar{c}_{ij}$ are listed in each plot. Lower row: Same as top but using the stiff-sand model.

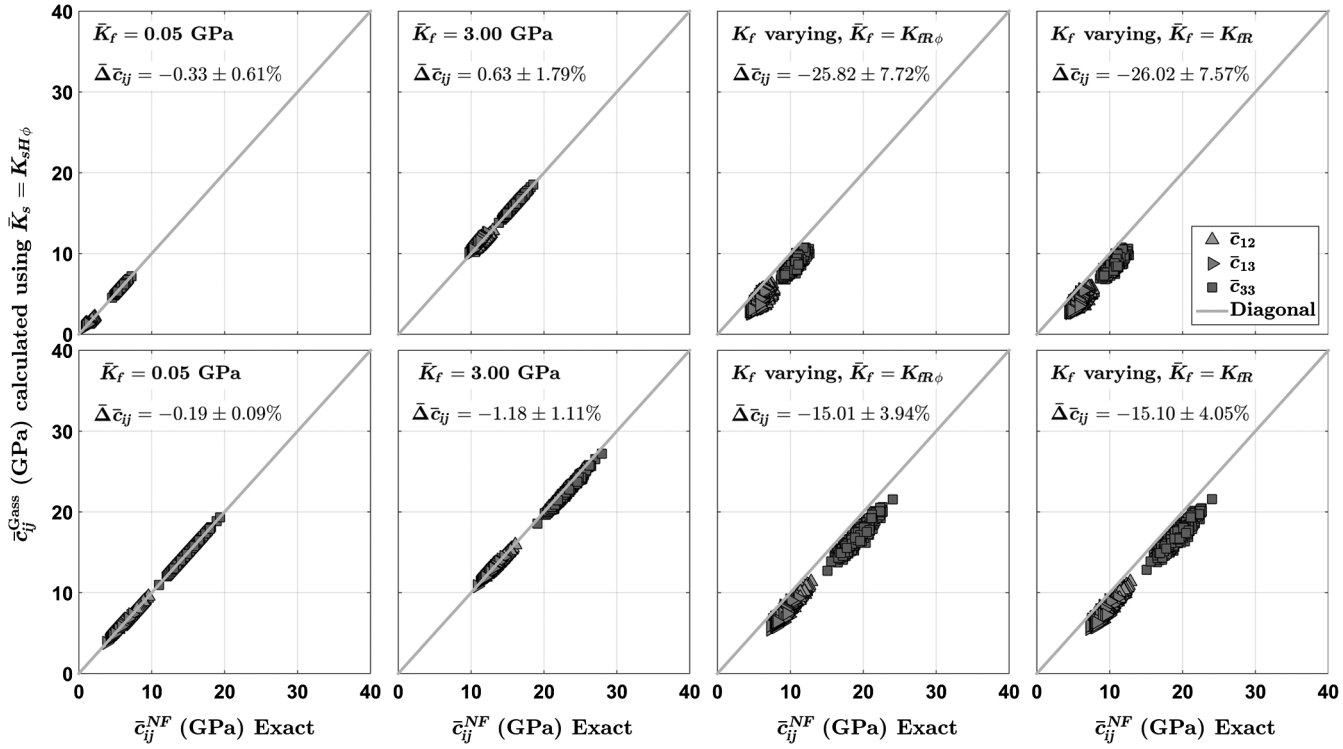


Figure 3. Same as Figure 2, but for hydraulically isolated layers.

the average relative error between the exact and the approximated solution stiffnesses. These approximations produced an average relative error of approximately $0.06 \pm 2.97\%$ for layers modeled with the soft-sand model and $-0.39 \pm 1.69\%$ for layers modeled with the stiff-sand model.

For a simple analytical approximation for $\bar{K}_f$ to be used in both models, we used the following linear combination:

$$K_{fRV\phi} = \frac{1}{4} K_{fR\phi} + \frac{3}{4} K_{fV\phi}, \tag{14}$$

and calculated $\bar{c}_{ij}^{\text{Gass}}$ assuming $\bar{K}_f = K_{fRV\phi}$ and compared them with the exact $\bar{c}_{ij}^{\text{NF}}$ (third column).

The relative errors listed in Figure 4 hold even for strong elastic contrast (up to 30% relative to the average values) in the dry-frame and mineral stiffnesses between the layers.

In the above examples, we used separately the soft- and stiff-sand models. If we randomly vary the model that will assign the dry elastic properties to a layer in the package (i.e., either soft- or stiff-sand models) and take $\bar{K}_s = K_{sH\phi}$, the results for the case of communicating layers having $\bar{K}_f = K_{fR\phi}$ produce a relative error of less than 1%. For the case of hydraulic isolation between layers, the empirically determined coefficients used to obtain $\bar{K}_f$ were $a = 0.23$ and $b = 0.81$, which produced a relative error of $-0.23 \pm 3.34\%$.

## $K_f$ FREQUENCY DISPERSION

We have shown that the effective fluid bulk modulus to be used in Gassmann's fluid substitution depends on the conditions of hydraulic communication between the layers filled with different fluids. In case of full communication (zero-frequency limit), $\bar{K}_f$ is smaller than in case of hydraulically isolated layers (infinite-frequency limit). With the same effective porosity (equation 4) and effective mineral bulk modulus (equation 9), we can use the anisotropic Gassmann's fluid substitution for the entire heterogeneous layered package for both frequency limits by simply changing $\bar{K}_f$. It is given in equation 11 for low-frequency limit and equation 14 for the high-frequency limit. This suggests that we can describe the frequency dependence of the global response by introducing the effective fluid bulk modulus versus frequency dispersion (Figure 5). In Figure 5, we connected the low- and high-frequency end members for $\bar{K}_f$ with a hypothetical curve using the standard linear solid functional form. The critical frequency at which the transition from the low- to high-frequency behavior occurs depends on many concrete variables, such as porosity, permeability, and viscosity. This is why the frequency dispersion curve shown is conceptual and the frequency values are not shown.

This concept of the fluid bulk modulus versus frequency dispersion was used by Christensen and Olsen (1994) to quantify the frequency dependence of the adiabatic bulk modulus of glycerol. Later, Vogelaar and Smeulders (2009) introduce the frequency dependence of the effective modulus of a gas bubble (dynamic pore-fluid modulus) in the context of White's (1975) poroelastic solu-

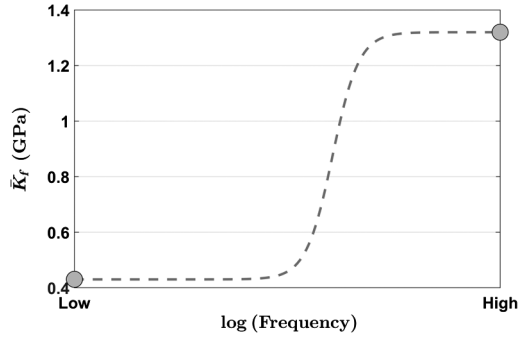


Figure 5. Apparent frequency dependence of the effective bulk modulus of the pore fluid for the entire composite. This dispersion curve is conceptual, connecting the low- and high-frequency endpoints with a standard linear solid curve. This is why specific frequency numbers are not shown.

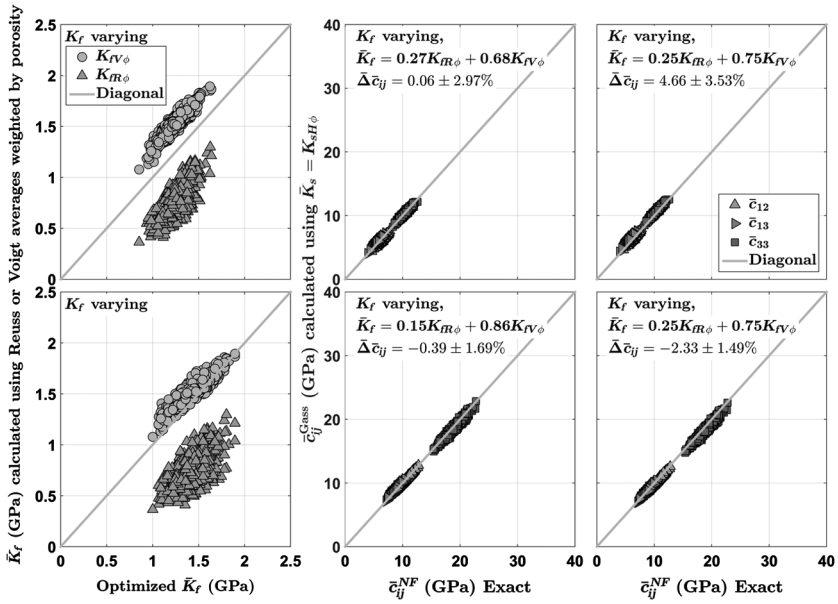


Figure 4. Hydraulically isolated layers. (Left column) The effective fluid bulk modulus computed from individual values using porosity-weighted Voigt (circles) and Reuss (triangles) averages. (Right column) Three $\bar{c}_{ij}^{\text{Gass}}$ from anisotropic Gassmann's fluid substitution computed using the Hill's average $K_{sH\phi}$ and $\bar{K}_f$ obtained from the combination of Voigt and Reuss averages weighted by porosity, respectively. The average relative errors and their respective standard deviations in percentage $\bar{\Delta}\bar{c}_{ij}$ are listed in the center and right columns. Upper row: The soft-sand model. Lower row: The stiff-sand model.

tion. Yao et al. (2015) use it to describe the effect of local squirt flow on the velocity-frequency dispersion in wet rock.

## WEAK CONTRAST APPROXIMATION: GASSMANN FORM

### Hydraulically communicating layers

Following the same linearization approach as described in Bakulin (2003) and Bakulin and Grechka (2003), we can simplify the exact poroelastic Backus solution by assuming

$$|(\alpha^{(k)} - \langle\alpha\rangle)/\langle\alpha\rangle| \ll 1 \tag{15}$$

to arrive at the following equations:

$$\begin{aligned} &\bar{c}_{KL}^{\text{Gass}^*} = \bar{c}_{KL}^{\text{dry}} + \langle\alpha\rangle^2\langle M^{-1}\rangle^{-1}; \quad K, L = 1, 2, 3, \\ &\bar{c}_{44}^{\text{Gass}^*} = \bar{c}_{44}^{\text{dry}}; \quad \bar{c}_{66}^{\text{Gass}^*} = \bar{c}_{66}^{\text{dry}}, \\ &\alpha = 1 - K_{\text{dry}}/K_s; \quad M = \left[\frac{\phi}{K_f} + \frac{\alpha - \phi}{K_s}\right]^{-1}. \end{aligned} \tag{16}$$

This form is analogous to the anisotropic Gassmann's fluid substitution equation (equation 5). Furthermore, if we impose additional constraints on the contrasts among the layers, namely

$$\begin{aligned} |(K_{\text{dry}}^{(k)} - \langle K_{\text{dry}}\rangle)/\langle K_{\text{dry}}\rangle| \ll 1, \\ |(\mu_{\text{dry}}^{(k)} - \langle \mu_{\text{dry}}\rangle)/\langle \mu_{\text{dry}}\rangle| \ll 1, \end{aligned} \tag{17}$$

where $\mu_{\text{dry}}$ is the shear modulus that is independent of the pore fluid, equation 16 reduces to the isotropic Gassmann form

$$K^{\text{Gass}^*} = \langle K_{\text{dry}}\rangle + \langle\alpha\rangle^2\langle M^{-1}\rangle^{-1}, \tag{18}$$

where the saturated effective medium is considered isotropic having bulk modulus $K^{\text{Gass}^*}$.

### Hydraulically isolated layers

Using the constraints presented in equations 15 and 17, as well as requiring

$$|(H^{(k)} - \langle H\rangle)/\langle H\rangle| \ll 1, \tag{19}$$

with $H = K_{\text{dry}} + 4\mu_{\text{dry}}/3 + \alpha^2 M$, we reduce the exact solution to the isotropic Gassmann form (neglecting the $\langle\alpha\rangle^n, n > 2$ terms),

$$K^{\text{sat}^*} = \langle K_{\text{dry}}\rangle + \langle\alpha^2 M\rangle. \tag{20}$$

It is important to note that although equations 18 and 20 have the same form, the fluid-dependent term $M$ in equations 18 and 20 is averaged differently depending on the state of hydraulic communication among layers. This difference in averaging makes the effective fluid in the hydraulic isolation case stiffer than in the full hydraulic communication case.

## DISCUSSION

The essence of the question we address here is determining the effective porosity, dry-frame stiffnesses, and solid and fluid bulk moduli that can be used as inputs in anisotropic Gassmann's fluid substitution equation to arrive at the effective stiffnesses of a heterogeneous finely layered package. To satisfy this requirement, we need to separately match three elastic stiffnesses. These are three independent equations that can be resolved in terms of three unknowns.

Instead of selecting these three unknowns, we simplify the problem by assuming that the effective porosity is the volume-averaged porosity and the effective dry-frame stiffnesses are the Backus averages of the individual elastic constants. We are left with only two unknowns, the effective $K_s$ and $K_f$. To obtain the former, we fill all layers with the same fluid, whose $K_f$ is now the effective fluid bulk modulus for the entire package (i.e., $\bar{K}_f = K_f$). Then, we find a single unknown $K_s$ from three independent equations. Naturally, we end up with three different answers. To address the overdetermined system, we postulate that the effective mineral bulk modulus $\bar{K}_s$ is the Hill's average of individual moduli weighted by the mineral fraction and test whether this selection is appropriate. By testing this assumption on many numerical simulation, we determine that it is plausible indeed (less than 2% average relative difference between exact and approximate stiffness values).

Next, we use this $\bar{K}_s$ to obtain $\bar{K}_f$ by saturating the layers with different fluids. Once again, we face an over-determined system of equations. An approximate solution for hydraulically communicating layers is the porosity-weighted Reuss average for $\bar{K}_f$ (less than 1% average relative difference).

The situation becomes more complicated in which the layers are hydraulically isolated. Hill's average for $K_s$ is still appropriate (less than 2% relative difference between exact and approximate stiffness values) but, as expected, the porosity-weighted Reuss average for $K_f$ is not. The appropriate approximation for $\bar{K}_f$ in this case is given in equation 14 (less than 6% average relative difference).

Let us mention here that there is another method of determining the effective solid and fluid properties of a layered package, not related to Gassmann's fluid substitution. We could have posed the question differently: What are the hypothetical uniform $\bar{K}_s$ and $\bar{K}_f$ to be assigned to each layer such that the poroelastic Backus average will give the same effective stiffnesses as the exact solution? It is interesting that using the $\bar{K}_s$ and $\bar{K}_f$ given in equations 9, 10, and 14 approximately satisfy this condition as well (Appendix B).

These results are aimed at providing an element of well-data-based seismic forward modeling eventually to be used in interpretation. Although hydraulic communication is likely to be nonexistent between sand and shale due to the low permeability of the former, it certainly can occur between two permeable sand layers saturated with different fluids. Our main finding is that depending on the frequency of investigation, one should use different fluid bulk modulus, the one given in equation 10 at low (seismic) frequency and in equation 14 at higher (logging) frequency. A step-by-step example of conducting frequency-dependent fluid substitution on a hypothetical two-layer system of sand with gas and fully brine-saturated sand is given in Appendix C. The result indicates that although the vertical P-wave velocity at the logging fre-

quency is 2.30 km/s, the respective velocity at the seismic frequency is 2.05 km/s, a 0.25 km/s difference to be accounted for in forward modeling. In addition, the respective P-wave impedance difference is 11%, which may alter the reflectivity.

One of the immediate applications of our results is synthetic seismic modeling. A recent example of such usage of somewhat similar basic science results is provided in Bryndzia et al. (2016). We also feel that in light of the results of our current work, direct interpretation of seismically derived impedances for porosity, lithology, and pore fluid is possible as well. An example of such a workflow is given in Arévalo-López and Dvorkin (2016). The authors did not have to use the principle of upscaled pore-fluid modulus, as the hydrocarbon present was low Gas to Oil Ratio (GOR) with the compressibility fairly close to that of the formation brine. The situation becomes more complicated when dealing with gas. This is an ongoing research to be conducted based on the results of the current paper.

## CONCLUSIONS

The specific issue addressed here is: What are the effective parameters to be used in Gassmann's fluid substitution if applied to a package of layers, and this package is treated as a homogeneous medium? In general, it is an issue of upscaling the parameters of a rock-physics operator. The concrete situation examined here is for the transform being Gassmann's fluid substitution and the composite being a finely layered package. The answer is that, strictly speaking, this transform is not applicable to the entire package. However, we find expressions for the effective parameters to be used in anisotropic Gassmann's transform that provide good approximation to the effective anisotropic stiffnesses from the exact solutions. This result can lead to apply the fluid substitution transform at a coarse scale of seismic resolution that accounts for hydraulic interaction inside the volume. It can also help in blocking various intervals in well data and making them suitable for forward seismic modeling.

Finally, by examining two limiting cases of very low and very high frequency, we find that the same Gassmann's transform can be used in both cases by introducing frequency dispersion to the fluid bulk modulus (dynamic pore fluid modulus).

## ACKNOWLEDGMENTS

This material is based on work supported by the U.S. Department of Energy, Office of Science, and Office of Basic Energy Sciences under Award Number DE-FG02-03ER15423. We thank G. Mavko for insightful discussions. Finally, we are grateful to the editors for their helpful comments and suggestions.

## APPENDIX A

## POROELASTIC BACKUS AVERAGING

### Quasi-static limit

The equations given by Gelinsky and Shapiro (1997) for the effective stiffness constants at the quasi-static limit for finely layered poroelastic isotropic media with $x_3$-direction as the axis of layering symmetry are

$$\begin{aligned}
\bar{c}_{12}^{\mathrm{QS}} &= 2\left\langle \frac{\lambda_{\mathrm{dry}}\mu_{\mathrm{dry}}}{\lambda_{\mathrm{dry}}+2\mu_{\mathrm{dry}}}\right\rangle + \left\langle \frac{\lambda_{\mathrm{dry}}}{\lambda_{\mathrm{dry}}+2\mu_{\mathrm{dry}}}\right\rangle^2 \left\langle \frac{1}{\lambda_{\mathrm{dry}}+2\mu_{\mathrm{dry}}}\right\rangle^{-1} + \frac{P^2}{R},\\
\bar{c}_{33}^{\mathrm{QS}} &= \left\langle \frac{1}{\lambda_{\mathrm{dry}}+2\mu_{\mathrm{dry}}}\right\rangle^{-1} + \frac{Q^2}{R},\\
\bar{c}_{13}^{\mathrm{QS}} &= \left\langle \frac{1}{\lambda_{\mathrm{dry}}+2\mu_{\mathrm{dry}}}\right\rangle^{-1} \left\langle \frac{\lambda_{\mathrm{dry}}}{\lambda_{\mathrm{dry}}+2\mu_{\mathrm{dry}}}\right\rangle + \frac{PQ}{R},\\
\bar{c}_{44}^{\mathrm{QS}} &= \langle(\mu_{\mathrm{dry}})^{-1}\rangle^{-1},\\
\bar{c}_{66}^{\mathrm{QS}} &= \langle\mu_{\mathrm{dry}}\rangle,\\
P &= -R\left(2\left\langle \frac{\alpha\mu_{\mathrm{dry}}}{\lambda_{\mathrm{dry}}+2\mu_{\mathrm{dry}}}\right\rangle + \left\langle \frac{\alpha}{\lambda_{\mathrm{dry}}+2\mu_{\mathrm{dry}}}\right\rangle \left\langle \frac{\lambda_{\mathrm{dry}}}{\lambda_{\mathrm{dry}}+2\mu_{\mathrm{dry}}}\right\rangle \right.\\
&\quad \left. \times \left\langle \frac{1}{\lambda_{\mathrm{dry}}+2\mu_{\mathrm{dry}}}\right\rangle^{-1}\right),\\
Q &= -R\left\langle \frac{\alpha}{\lambda_{\mathrm{dry}}+2\mu_{\mathrm{dry}}}\right\rangle \left\langle \frac{1}{\lambda_{\mathrm{dry}}+2\mu_{\mathrm{dry}}}\right\rangle^{-1},\\
R &= \left[\langle M^{-1}\rangle \left\langle \frac{\alpha^2}{\lambda_{\mathrm{dry}}+2\mu_{\mathrm{dry}}}\right\rangle - \left\langle \frac{\alpha}{\lambda_{\mathrm{dry}}+2\mu_{\mathrm{dry}}}\right\rangle^2 \left\langle \frac{1}{\lambda_{\mathrm{dry}}+2\mu_{\mathrm{dry}}}\right\rangle^{-1}\right]^{-1}.
\end{aligned} \tag{A-1}$$

The subscript dry denotes elastic moduli at drained conditions, $\alpha = 1 - K_{\mathrm{dry}}/K_s$ is the Biot and Willis (1957) parameter with $K_s$ being the bulk modulus of the grain mineral and $\langle\cdot\rangle$ is the averaging operator across all layers. For isotropic layers, we have $K_{\mathrm{dry}} = \lambda_{\mathrm{dry}} + 2\mu_{\mathrm{dry}}/3$. The poroelastic parameter $M$ is expressed as

$$M = \left[\frac{\phi}{K_f} + \frac{\alpha-\phi}{K_s}\right]^{-1}, \tag{A-2}$$

where $\phi$ is the porosity and $K_f$ is the pore fluid's bulk modulus. By definition of $M$, it is assumed that each layer within a model is composed of a single mineral.

Drained effective stiffness matrix $\bar{c}_{lm}^{\mathrm{dry}}$ is obtained through equation A-1 by omitting fluid-related terms (i.e., $R = 0$), which is essentially an elastic Backus averaging on the drained elastic components.

### No-flow limit

The equations for the elastic stiffnesses at the no-flow limit for finely layered media are,

$$\begin{aligned}
\bar{c}_{12}^{\mathrm{NF}} &= 2\left\langle \frac{(H-2\mu_{\mathrm{dry}})\mu_{\mathrm{dry}}}{H}\right\rangle + \left\langle \frac{H-2\mu_{\mathrm{dry}}}{H}\right\rangle^2 \left\langle \frac{1}{H}\right\rangle^{-1},\\
\bar{c}_{33}^{\mathrm{NF}} &= \left\langle \frac{1}{H}\right\rangle^{-1},\\
\bar{c}_{13}^{\mathrm{NF}} &= \left\langle \frac{1}{H}\right\rangle^{-1} \left\langle \frac{H-2\mu_{\mathrm{dry}}}{H}\right\rangle,\\
\bar{c}_{44}^{\mathrm{NF}} &= \langle(\mu_{\mathrm{dry}})^{-1}\rangle^{-1},\\
\bar{c}_{66}^{\mathrm{NF}} &= \langle\mu_{\mathrm{dry}}\rangle,
\end{aligned} \tag{A-3}$$

with

$$H = \lambda_{\mathrm{dry}} + 2\mu_{\mathrm{dry}} + \alpha^2 M, \tag{A-4}$$

which is the undrained P-wave modulus for an isotropic, homogeneous, linearly elastic composite of Gassmann's fluid substitution.

### Special case: Uniform $K_s$ in all layers

When the mineral bulk moduli of all layers within a package are equal, we show that the poroelastic Backus averaging devolve into Gassmann's anisotropic fluid substitution formula. For ease of notation, let $E_G = \lambda_{\rm dry} + 2\mu_{\rm dry}$ be the dry-rock P-wave modulus. First, we rewrite $R$ from equation A-1 assuming $K_s$ is constant and using $\alpha = 1 - K_{\rm dry}/K_s$ to obtain

$$R^* = \left[\langle M^{-1}\rangle + \frac{1}{K_s^2}\left\langle\frac{K_{\rm dry}^2}{E_G}\right\rangle - \frac{1}{K_s^2}\left\langle\frac{K_{\rm dry}}{E_G}\right\rangle^2\left\langle\frac{1}{E_G}\right\rangle^{-1}\right]^{-1},$$
$$= \left[\left\langle\frac{\phi}{K_f}\right\rangle + \frac{1-\frac{1}{K_s}\left(\langle K_{\rm dry}\rangle - \left\langle\frac{K_{\rm dry}^2}{E_G}\right\rangle + \left\langle\frac{K_{\rm dry}}{E_G}\right\rangle^2\left\langle\frac{1}{E_G}\right\rangle^{-1}\right) - \langle\phi\rangle}{K_s}\right]^{-1}. \quad \text{(A-5)}$$

Using the relation in equation 5, we would show that

$$\sum_{K=1}^{3}\sum_{L=1}^{3}\bar{c}_{KL}^{\rm dry} = 9\left(\langle K_{\rm dry}\rangle - \left\langle\frac{K_{\rm dry}^2}{E_G}\right\rangle + \left\langle\frac{K_{\rm dry}}{E_G}\right\rangle^2\left\langle\frac{1}{E_G}\right\rangle^{-1}\right),$$
$$= 12\left\langle\frac{\lambda_{\rm dry}\mu_{\rm dry}}{E_G}\right\rangle + 8\left\langle\frac{\mu_{\rm dry}^2}{E_G}\right\rangle + 9\left\langle\frac{\lambda_{\rm dry}+2\mu_{\rm dry}/3}{E_G}\right\rangle^2\left\langle\frac{1}{E_G}\right\rangle^{-1},$$
$$= 12\left\langle\frac{\lambda_{\rm dry}\mu_{\rm dry}}{E_G}\right\rangle + 8\left\langle\frac{\mu_{\rm dry}^2}{E_G}\right\rangle + \left\langle\frac{3\lambda_{\rm dry}+2\mu_{\rm dry}}{E_G}\right\rangle^2\left\langle\frac{1}{E_G}\right\rangle^{-1}. \quad \text{(A-6)}$$

Indeed, explicitly writing the left side, we obtain

$$\sum_{K=1}^{3}\sum_{L=1}^{3}\bar{c}_{KL}^{\rm dry} = 12\left\langle\frac{\lambda_{\rm dry}\mu_{\rm dry}}{E_G}\right\rangle + 8\left\langle\frac{\mu_{\rm dry}^2}{E_G}\right\rangle + 4\left(\left\langle\frac{\lambda_{\rm dry}}{E_G}\right\rangle + \frac{1}{2}\right)^2\left\langle\frac{1}{E_G}\right\rangle^{-1},$$
$$= 12\left\langle\frac{\lambda_{\rm dry}\mu_{\rm dry}}{E_G}\right\rangle + 8\left\langle\frac{\mu_{\rm dry}^2}{E_G}\right\rangle + 4\left\langle\frac{2\lambda_{\rm dry}+E_G}{2E_G}\right\rangle^2\left\langle\frac{1}{E_G}\right\rangle^{-1},$$
$$= 12\left\langle\frac{\lambda_{\rm dry}\mu_{\rm dry}}{E_G}\right\rangle + 8\left\langle\frac{\mu_{\rm dry}^2}{E_G}\right\rangle + \left\langle\frac{3\lambda_{\rm dry}+2\mu_{\rm dry}}{E_G}\right\rangle^2\left\langle\frac{1}{E_G}\right\rangle^{-1}. \quad \text{(A-7)}$$

Therefore, $R^*$ can be written as

$$R^* = \left[\left\langle\frac{\phi}{K_f}\right\rangle + \frac{1 - \frac{\sum_{K=1}^{3}\sum_{L=1}^{3}\bar{c}_{KL}^{\rm dry}}{9K_s} - \langle\phi\rangle}{K_s}\right]^{-1}, \quad \text{(A-8)}$$

resembling the form of $\bar{M}$ in equation 5. Similarly, the $Q$ term in equation A-1 can be expanded to obtain

$$Q^* = -R\left\langle\frac{1-\frac{K_{\rm dry}}{K_s}}{E_G}\right\rangle\left\langle\frac{1}{E_G}\right\rangle^{-1},$$
$$= -R\left[\left(\left\langle\frac{1}{E_G}\right\rangle - \frac{1}{K_s}\left\langle\frac{K_{\rm dry}}{E_G}\right\rangle\right)\left\langle\frac{1}{E_G}\right\rangle^{-1}\right],$$
$$= -R\left[1 - \frac{1}{K_s}\left\langle\frac{K_{\rm dry}}{E_G}\right\rangle\left\langle\frac{1}{E_G}\right\rangle^{-1}\right]. \quad \text{(A-9)}$$

The terms in the bracket are equivalent to $\beta_3$ in equation 5 because

$$\beta_3 = 1 - \frac{c_{13}+c_{23}+c_{33}}{3K_s},$$
$$= 1 - \frac{1}{3K_s}\left(2\left\langle\frac{\lambda_{\rm dry}}{E_G}\right\rangle\left\langle\frac{1}{E_G}\right\rangle^{-1} + \left\langle\frac{1}{E_G}\right\rangle^{-1}\right),$$
$$= 1 - \frac{1}{3K_s}\left(\left\langle\frac{1}{E_G}\right\rangle^{-1}\left\langle\frac{3E_G}{E_G}\right\rangle\right),$$
$$= 1 - \frac{1}{K_s}\left\langle\frac{K_{\rm dry}}{E_G}\right\rangle\left\langle\frac{1}{E_G}\right\rangle^{-1}. \quad \text{(A-10)}$$

Similarly, one can show that $\beta_1 = \beta_2 = (-P/R)$. We conclude that the poroelastic Backus averaging is reduced to anisotropic Gassmann's fluid substitution form (equation 5) given $K_s$ is uniform within the layered package.

## APPENDIX B

## EFFECTIVE $K_f$ AND $K_s$ USING POROELASTIC BACKUS AVERAGING EQUATIONS

Here, we duplicate the results obtained under the requirement that instead of making the poroelastic Backus averaging consistent with Gassmann's fluid substitution scheme, we make it consistent with the poroelastic Backus averaging itself by using "effective" bulk moduli of the solid and fluid. The question here is: What should be the homogeneous $\bar{K}_s$ and $\bar{K}_f$ that could replace the heterogeneous elemental values to arrive at approximately the same result as given by the exact poroelastic Backus equations for full-hydraulic communication and complete hydraulic isolation cases? To address this question, we repeated the same computational experiments as described in the main text. The results are shown in Figures B-1–B-4 and are analogous to the respective figures in the main text.

It is interesting that the results for $\bar{K}_s$ and $\bar{K}_f$ obtained under the Gassmann-consistency requirement hold in this case. This is likely

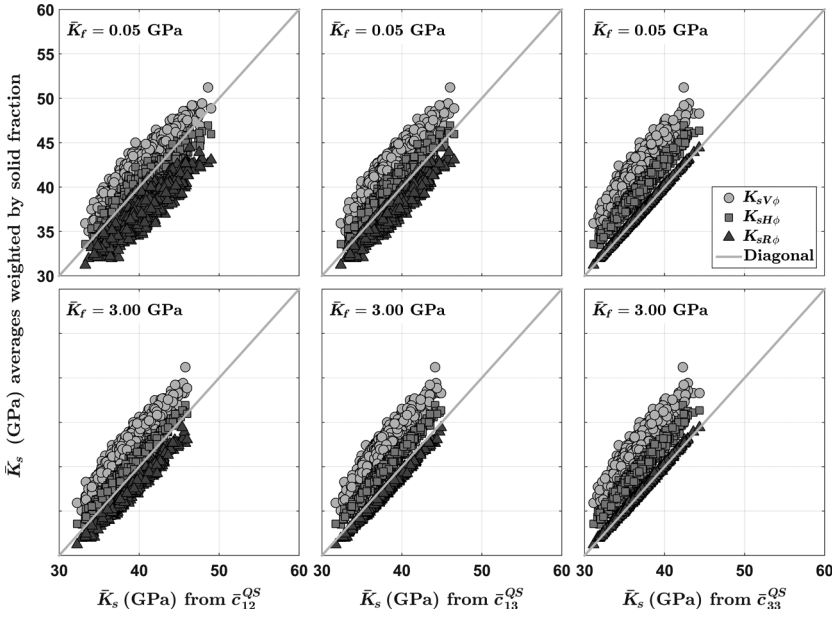


Figure B-1. Same as Figure 1, but for the consistency requirements examined here.

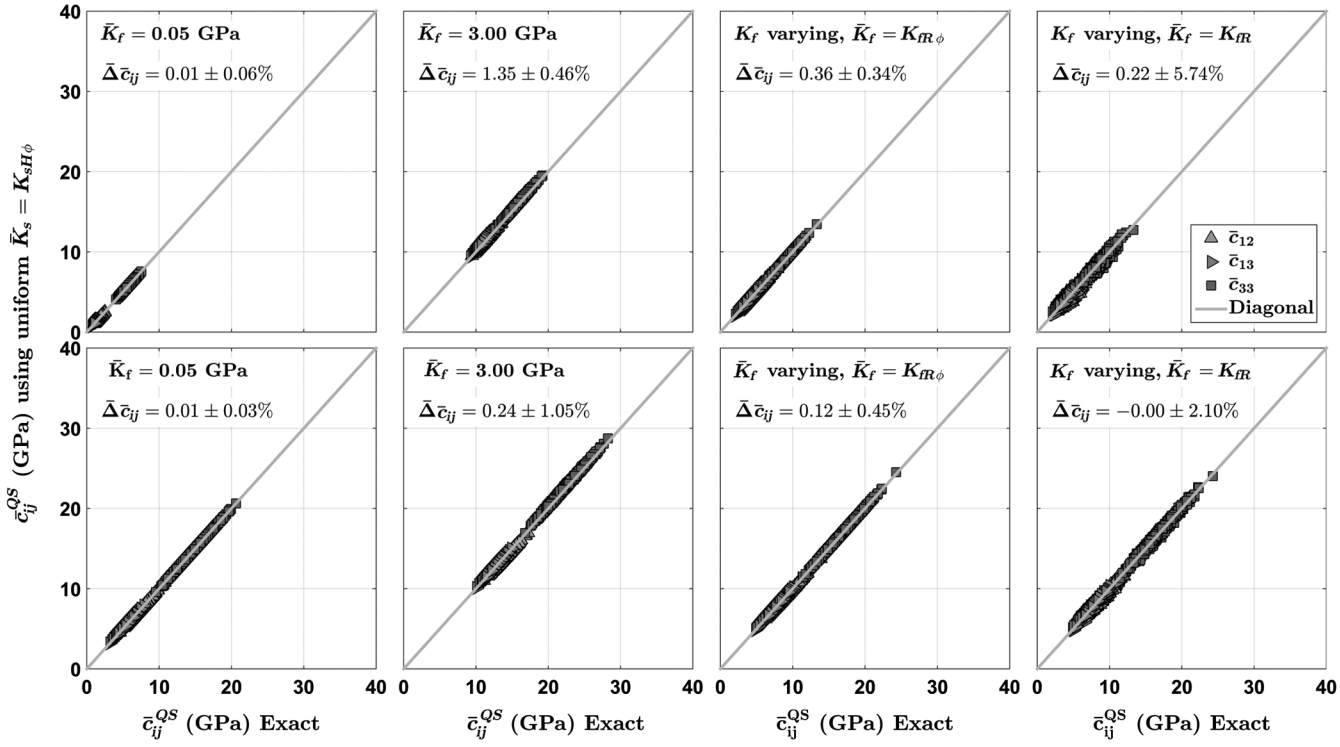


Figure B-2. Same as Figure 2, but for the consistency requirements examined here.

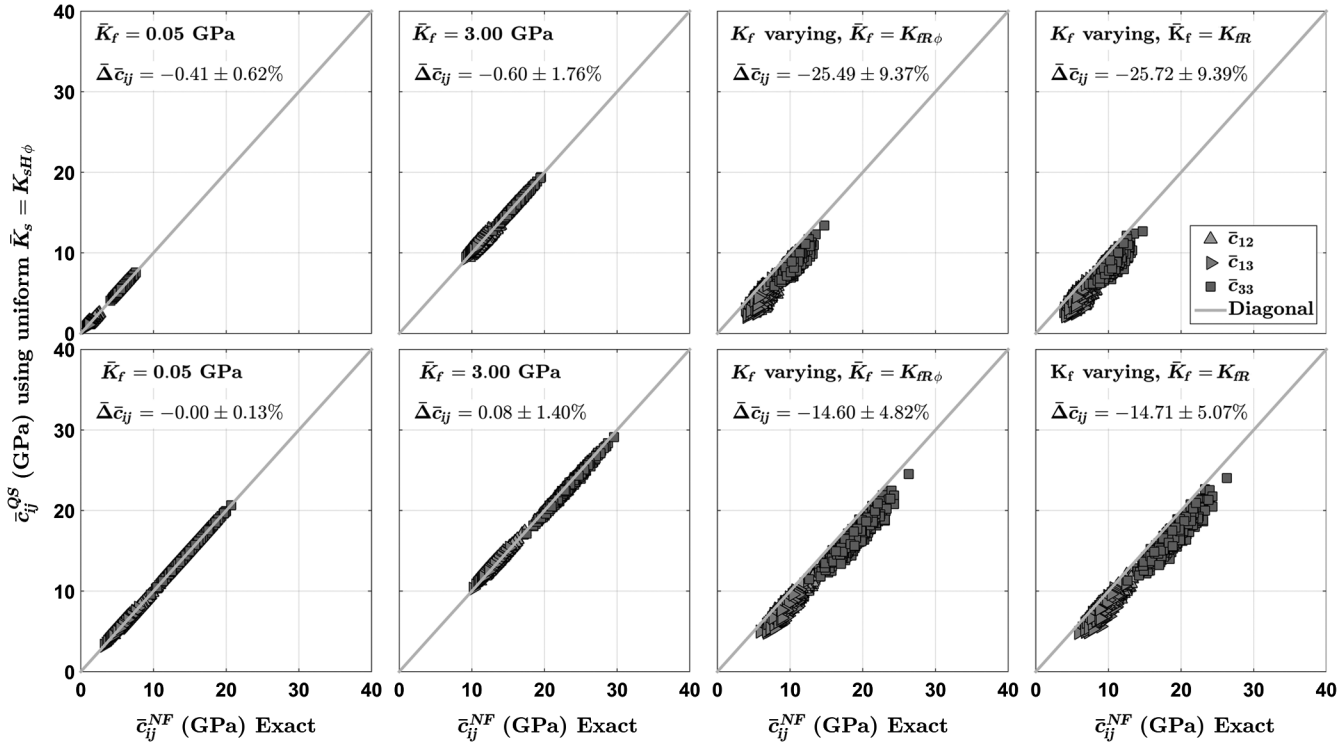


Figure B-3. Same as Figure 3, but for the consistency requirements examined here.

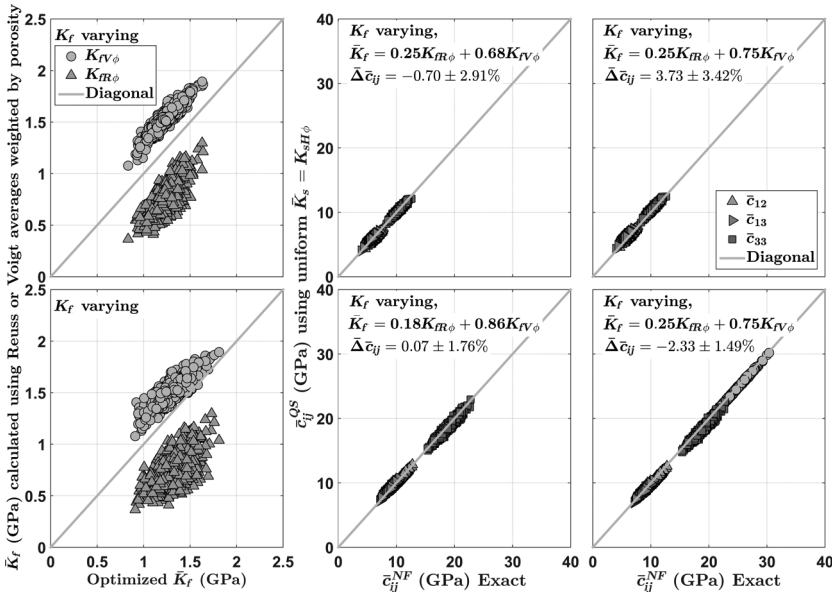


Figure B-4. Same as Figure 4, but for the consistency requirements examined here.

because, as shown in the main text, the poroelastic Backus equations degenerate to anisotropic (or isotropic) Gassmann's equations if the contrast between the layers is small. Apparently, this result is approximately correct even for the high-contrast case.

## APPENDIX C

## STEP-BY-STEP EXAMPLE OF ANISOTROPIC GASSMANN'S FLUID SUBSTITUTION AT VARYING FREQUENCY

Consider a two-layer system of high-porosity sand. The upper layer has 20% water saturation, whereas the lower layer is fully water saturated. The thickness of each layer is 15 cm. The mineralogy is quartz and clay. The elastic properties of the layers are computed using the soft-sand model (Mavko et al., 2009). The parameters of the layers are listed in Table C-1.

Assume that the viscosity of water $\eta$ is 1 cPs $= 10^{-3}$ Pa s, and the permeability $\kappa$ of the layers is 500 and 200 mD in the upper and lower layer, respectively. The diffusion length computed as $L \approx 2\sqrt{\kappa K_f/(\eta\phi f)}$ (Mavko et al., 2009) is approximately 60 cm at $f =$ 20 Hz (seismic) and 3 cm at $f = 10$ kHz (logging), meaning that the layers will not communicate at the logging frequency but will communicate at seismic frequency. The effective bulk density $\bar{\rho}_b$ and porosity are the volume averages of the respective individual values. The effective bulk modulus of the mineral phase is computed from equation 9 (porosity-weighted Hill's average). The effective dry-rock stiffness matrix is computed using the elastic Backus average of the individual dry-rock elastic moduli (equation A-1). The low-frequency effective fluid bulk modulus is the porosity-weighted harmonic average of the individual moduli according to equation 10 (0.09 GPa), whereas that for high frequency is according to equation 14 (1.04 GPa). By conducting anisotropic Gassmann fluid substitution (equation 5), we find that the low-frequency effective stiffness $\bar{c}_{33}^{\text{Gass}}$ is 8.43 GPa, whereas its high-frequency counterpart is 10.55 GPa, indicating a noticeable difference. The respective P-wave velocity $V_{\text{P}} = \sqrt{\bar{c}_{33}^{\text{Gass}}/\bar{\rho}_b}$ in the vertical direction is 2.05 and 2.30 km/s. The former value should be used for well-data upscaling for seismic modeling. This difference is the result of the difference in $\bar{K}_f$ (0.09 versus 1.04 GPa). The former reflects the effective fluid property behind a recorded seismic amplitude. In addition, the difference in P-wave impedance $I_P = \rho_b V_{\text{P}}$ between the low- and high-frequency cases is 11%, which may alter the reflectivity.

**Table C-1. Inputs for the effective elastic properties computation in this example. Starting with the second column: porosity, clay content, pore fluid bulk modulus, bulk density, and the P- and S-wave velocities according to the soft-sand model.**

| Layer | $\phi$ | $C$ | $K_f$ (GPa) | $\rho_b$ (g/cm$^3$) | $V_{\text{P}}$ (km/s) | $V_{\text{S}}$ (km/s) |
|---|---|---|---|---|---|---|
| 1 | 0.35 | 0.00 | 0.052 | 1.84 | 1.78 | 1.22 |
| 2 | 0.30 | 0.05 | 2.86 | 2.17 | 2.53 | 1.21 |

## REFERENCES


Arévalo-López, H. S., and J. P. Dvorkin, 2016, Porosity, mineralogy, and pore fluid from simultaneous impedance inversion: The Leading Edge, **35**, 423–429, doi: 10.1190/tle35050423.1.

Avseth, P., T. Mukerji, T. Jørstad, G. Mavko, and T. Veggeland, 2001, Seismic reservoir mapping from 3D AVO in a North Sea turbidite system: Geophysics, **66**, 1157–1176, doi: 10.1190/1.1487063.

Avseth, P., T. Mukerji, and G. Mavko, 2005, Quantitative seismic interpretation: Applying rock physics tools to reduce interpretation risk: Cambridge University Press.

Backus, G. E., 1962, Long-wave elastic anisotropy produced by horizontal layering: Journal of Geophysical Research, **67**, 4427–4440, doi: 10.1029/JZ067i011p04427.

Bakulin, A., 2003, Intrinsic and layer-induced vertical transverse isotropy: Geophysics, **68**, 1708–1713, doi: 10.1190/1.1620644.

Bakulin, A., and V. Grechka, 2003, Effective anisotropy of layered media: Geophysics, **68**, 1817–1821, doi: 10.1190/1.1635034.

Berryman, J. G., 1998, Transversely isotropic poroelasticity arising from thin isotropic layers, *in* K. M. Golden, G. R. Grimmett, R. D. James, G. W. Milton, and P. N. Sen, eds., Mathematics of multiscale materials: Springer, 37–50.

Berryman, J. G., 2011, Mechanics of layered anisotropic poroelastic media with applications to effective stress for fluid permeability: International Journal of Engineering Science, **49**, 122–139, doi: 10.1016/j.ijengsci.2010.06.027.

Biot, M. A., 1956a, Theory of propagation of elastic waves in a UID saturated porous solid. I: Low-frequency range: Journal of the Acoustical Society of America, **28**, 168–178, doi: 10.1121/1.1908239.

Biot, M. A., 1956b, Theory of propagation of elastic waves in a UID saturated porous solid. II: Higher-frequency range: Journal of the Acoustical Society of America, **28**, 179–191, doi: 10.1121/1.1908241.

Biot, M. A., 1962, Mechanics of deformation and acoustic propagation in porous media: Journal of the Acoustical Society of America, **33**, 1482–1498.

Biot, M. A., and D. Willis, 1957, The elastic coefficients of the theory of consolidation: Journal of Applied Mechanics, **24**, 594–601.

Bryndzia, L. T., N. Saxena, S. S. Dolan, M. G. Kittridge, M. L. Rosenquist, and N. Braunsdorf, 2016, Interpreting direct hydrocarbon indicators of low-API biodegraded oils a case study from a deepwater South Atlantic Basin: TLE, **35**, 511–515.

Christensen, T., and N. B. Olsen, 1994, Determination of the frequency-dependent bulk modulus of glycerol using a piezoelectric spherical shell: Physical Review B, **49**, 15396–15399, doi: 10.1103/PhysRevB.49.15396.

Dejtrakulwong, P., 2012, Rock physics and seismic signatures of sub-resolution sand-shale: Ph.D. thesis, Stanford University.
Dejtrakulwong, P., and G. Mavko, 2011, Fluid substitution for laminated sandshale sequences: 81st Annual International Meeting, SEG, Expanded Abstracts, 2183–2187.
Gassmann, F., 1951, Über die Elastizität poröser Medien: Vierteljahrsschrift der Natur- forschenden Gesellschaft in Zürich, **96**, 1–23.
Gelinsky, S., and S. A. Shapiro, 1997, Poroelastic Backus averaging for anisotropic layered fluid- and gas-saturated sediments: Geophysics, **62**, 1867–1878, doi: 10.1190/1.1444287.
Katahara, K. W., 2004, Fluid substitution in laminated shaly sands: 74th Annual International Meeting, SEG, Expanded Abstracts, 1718–1721.
Marion, D., T. Mukerji, and G. Mavko, 1994, Scale effects on velocity dispersion: From ray to effective-medium theories in stratified media: Geophysics, **59**, 1613–1619, doi: 10.1190/1.1443550.
Mavko, G., T. Mukerji, and J. Dvorkin, 2009, The rock physics handbook: Tools for seismic analysis in porous media (2nd ed.): Cambridge University Press.
Morlet, J., G. Arens, E. Fourgeau, and D. Giard, 1982, Wave propagation and sampling theory. Part I: Complex signal and scattering in multilayered media: Geophysics, **47**, 203–221, doi: 10.1190/1.1441328.
Postma, G. W., 1955, Wave propagation in a stratified medium: Geophysics, **20**, 780–806, doi: 10.1190/1.1438187.
Sams, M. S., 1995, Attenuation and anisotropy: The effect of extra fine layering: Geophysics, **60**, 1646–1655, doi: 10.1190/1.1443897.
Schoenberg, M., and F. Muir, 1989, A calculus for finely layered anisotropic media: Geophysics, **54**, 581–589, doi: 10.1190/1.1442685.
Schoenberger, M., and F. K. Levin, 1978, Apparent attenuation due to intrabed multiples: Geophysics, **43**, 730–737, doi: 10.1190/1.1440849.
Skelt, C., 2004, Fluid substitution in laminated sands: The Leading Edge, **23**, 485–493, doi: 10.1190/1.1756839.
Symes, W. W., 2008, Migration velocity analysis and waveform inversion: Geophysical Prospecting, **56**, 765–790, doi: 10.1111/j.1365-2478.2008.00698.x.
Thomsen, L., 1986, Weak elastic anisotropy: Geophysics, **51**, 1954–1966, doi: 10.1190/1.1442051.
Virieux, J., and S. Operto, 2009, An overview of full-waveform inversion in exploration geophysics: Geophysics, **74**, no. 6, WCC1–WCC26, doi: 10.1190/1.3238367.
Vogelaar, B. B. S. A., and D. M. J. Smeulders, 2009, Effective Biot theory for the speed and attenuation of seismic waves in saturated rocks containing small gas fractions, *in* H. I. Ling, A. Smyth, and R. Betti, eds., PoroMechanics IV: DEStech Publications Inc., 473–478.
White, J. E., 1975, Computed seismic speeds and attenuation in rocks with partial gas saturation: Geophysics, **40**, 224–232, doi: 10.1190/1.1440520.
Yao, Q., D. H. Han, F. Yan, and L. Zhao, 2015, Modeling attenuation and dispersion in porous heterogeneous rocks with dynamic fluid modulus: Geophysics, **80**, no. 3, D183–D194, doi: 10.1190/geo2013-0410.1.